

# Research on Influences of geometry parameters on floating-ring squeeze film damper

Yao Fu<sup>1</sup>, Guihuo Luo<sup>2</sup>

Nanjing University of Aeronautics and Astronautics, Nanjing, China

<sup>2</sup>Corresponding author

E-mail: <sup>1</sup>hengshuishifuyao@126.com, <sup>2</sup>ghluo@nuaa.edu.cn

(Accepted 14 September 2015)

**Abstract.** In this paper, numerical and experimental researches were conducted to explore dynamic characteristics of the floating-ring squeeze film damper. The influences of the eccentricity, radial clearance and width of oil film were considered. Reynolds equations of the inner and outer oil film were derived and solved by finite difference method and SOR-Newton method to obtain pressure distribution of the oil film and thus the equivalent stiffness and damping. Effectiveness of the numerical research was validated by experimental results.

**Keywords:** floating-ring squeeze film damper, dynamic characteristics, equivalent stiffness, equivalent damping.

## 1. Introduction

Squeeze film bearing dampers are lubricated elements providing viscous damping in mechanical systems. Squeeze film dampers in rotating machinery provide structural isolation, reduce the amplitudes of rotor response to imbalance, and in some instances, assist to suppress rotor dynamic instability [1].

Floating-ring squeeze film dampers (FSFD), which is more efficient than traditional SFD, has been applied in aeroengines to control excessive vibration levels of rotors [2] thus to suppress the nonlinear phenomena, such as amplitude jump and bistability. This, necessitates the study on influences of different geometry parameters on the dynamic characteristics of the FSFD.

Schematic of the FSFD applied in the work is presented in Fig. 1 [3]. FSFD has two layers of oil film, the inner film and the outer film, which are separated by the floating ring. The oil films were treated as centralizing springs and coupled dampers.

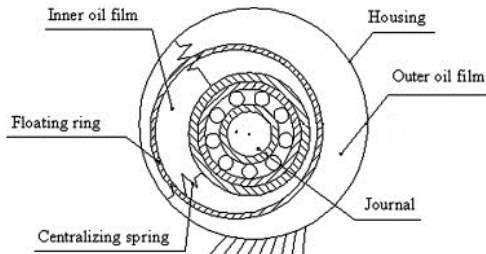


Fig. 1. Schematic of a floating-ring squeeze film damper

## 2. Basic theory

The simplified model of the FSFD is shown in Fig. 2. A small hexahedron is taken for analysis [4], as shown in Fig. 3. The coordinate system consists of three mutually perpendicular axis, X – the circumferential direction, Y – the radial direction and Z – the axial direction [5]. Only the forces acting on axis X were illustrated in Fig. 3. Radius of the journal was 14 mm and width of the oil film was 12.8 mm.

Eq. (1) can be obtained from force balance and Eq. (2) is obtained by simplification of Eq. (1) by neglecting the pressure gradient in radial direction. Integrating Eq. (2) twice, Eq. (3) is obtained.

$$\begin{cases} \frac{\partial p}{\partial X} = \frac{\partial \tau_{YX}}{\partial Y} + \frac{\partial \tau_{ZX}}{\partial Z}, \\ \frac{\partial p}{\partial Y} = \frac{\partial \tau_{XY}}{\partial X} + \frac{\partial \tau_{YZ}}{\partial Z}, \\ \frac{\partial p}{\partial Z} = \frac{\partial \tau_{XZ}}{\partial X} + \frac{\partial \tau_{YZ}}{\partial Y}, \end{cases} \quad (1)$$

where,  $p$  the pressure of oil,  $\tau_{YX}$  the tangential force on X-Z plane and pointed to the X axis direction,  $\tau_{ZX}$  the tangential force on X-Y plane and pointed to the X axis direction,  $\tau_{XY}$  the tangential force on Y-Z plane and pointed to the X axis direction,  $\tau_{XY}$  the tangential force on Y-Z plane and pointed to the Z axis direction,  $\tau_{XZ}$  the tangential force on Y-Z plane and pointed to the X axis direction,  $\tau_{YZ}$  the tangential force on X-Z plane and pointed to the Z axis direction.

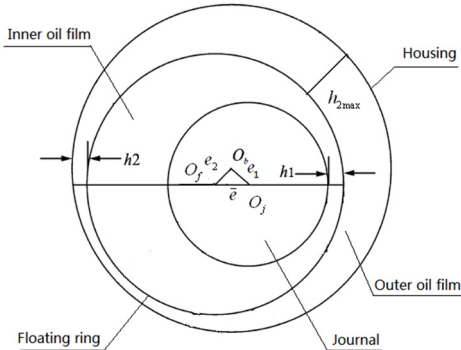


Fig. 2. The simplified model of FSFD

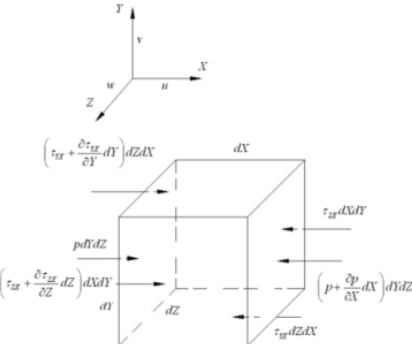


Fig. 3. An element of the oil film

$$\begin{aligned} \frac{\partial p}{\partial X} &= \frac{\partial}{\partial Y} \left( \mu \frac{\partial u}{\partial Y} \right), \\ \frac{\partial p}{\partial Z} &= \frac{\partial}{\partial Y} \left( \mu \frac{\partial w}{\partial Y} \right), \end{aligned} \quad (2)$$

where,  $\mu$  viscosity of the oil.

$$\begin{aligned} u &= \frac{1}{2\mu} \frac{\partial p}{\partial X} Y^2 + \frac{Y}{\mu} C_1 + C_2, \\ w &= \frac{1}{2\mu} \frac{\partial p}{\partial Z} Y^2 + \frac{Y}{\mu} C_3 + C_4, \end{aligned} \quad (3)$$

where,  $C_1, C_2, C_3, C_4$  are integration constants.

The Reynolds Equation, Eq. (4), can be derived by substituting Eq. (3) into the continuity equation of three-dimensional compressible flow.

$$\frac{\partial}{\partial X} \left( \frac{\rho h^3}{\mu} \frac{\partial p}{\partial X} \right) + \frac{\partial}{\partial Z} \left( \frac{\rho h^3}{\mu} \frac{\partial p}{\partial Z} \right) = 6(U_2 - U_1) \frac{\partial(\rho h)}{\partial X} + 12U_1 h \frac{\partial \rho}{\partial X} + 12\rho(V_1 - V_2) + 12h \frac{\partial \rho}{\partial t}, \quad (4)$$

where,  $\rho$  the density of the oil,  $h$  radial clearance,  $V_1$  the speed of journal in circumferential direction,  $V_2$  the speed of floating ring in circumferential direction,  $U_1$  the speed of journal in radial direction,  $U_2$  the speed of floating ring in radial direction.

Relative positions of journal, floating ring and housing were illustrated in Fig. 4.

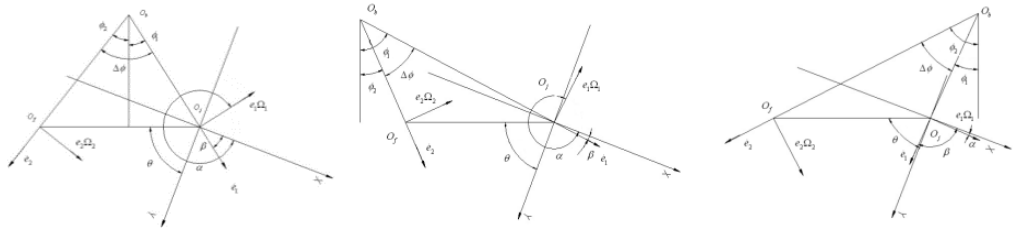


Fig. 4. Schematic of the center points relative position

Substituting the boundary conditions of inner and outer film into Eq. (4) to obtain Eq. (5) and Eq. (6).

$$\frac{1}{R_j^2} \frac{\partial}{\partial \theta} \left( \frac{h^3}{\mu} \frac{\partial p}{\partial \theta} \right) + \frac{\partial}{\partial Z} \left[ \frac{h^3}{\mu} \frac{\partial p}{\partial Z} \right] = 6 \left( e_1 \Omega_1 \sin(\theta - \phi_1) - R_{fi} \omega_1 - e_2 \Omega_2 \sin(\theta + \phi_2) \right) \frac{1}{R_j} \frac{\partial h}{\partial \theta} \quad (5)$$

$$+ 12 \left( -e_2 \Omega_2 \cos(\theta + \phi_2) + e_1 \Omega_1 \cos(\theta - \phi_1) \right),$$

where,  $\Omega_1$  the whirl speed of the journal,  $\Omega_2$  the whirl speed of the floating ring,  $R_j$  the radius of the journal,  $R_{fi}$  the inside radius of the floating ring and  $e_1, e_2, \theta, \phi_1, \phi_2$  were illustrated in Fig. 4.

$$\frac{1}{R_{fo}^2} \frac{\partial}{\partial \theta} \left( \frac{h_2^3}{\mu} \frac{\partial p}{\partial \theta} \right) + \frac{\partial}{\partial Z} \left[ \frac{h_2^3}{\mu} \frac{\partial p}{\partial Z} \right] = 6(\omega_1 - 2\Omega_2) \frac{\partial(h_2)}{\partial \theta}, \quad (6)$$

where,  $R_{fo}$  the outside radius of the floating ring,  $h_2$  the radial clearance of the outer film.

The spin speed of the floating ring can be derived by torque balance:

$$\int_0^{2\pi} \tau_n R_{fi} d\theta = \int_0^{2\pi} \tau_w R_{fo} d\theta, \quad (7)$$

with the short bearing assumption and Reynolds boundary condition, the pressure distribution of the oil film was obtained by finite difference method (FDM) and SOR-Newton iteration method. The grid for FDM is shown in Fig. 5 and Eqs. (8) and (9) are the iteration form of Eqs. (5) and (6).

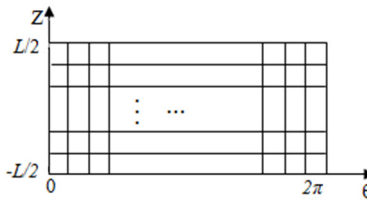


Fig. 5. The divided section of the FSFD

$$f = p_{i,j}A + p_{i+1,j}E + p_{i,j+1}N + p_{i-1,j}W + p_{i,j-1}S + Q = 0, \quad (8)$$

$$P_{i,j}^{k+1} = P_{i,j}^k - \omega \frac{f_{i,j}(P_{i-1,j}^{k+1}, P_{i,j-1}^{k+1}, P_{i,j}^k, P_{i+1,j}^k, P_{i,j+1}^k)}{\partial_{i,j} f_{i,j}(P_{i-1,j}^{k+1}, P_{i,j-1}^{k+1}, P_{i,j}^k, P_{i+1,j}^k, P_{i,j+1}^k)}. \quad (9)$$

### 3. Influences of geometry parameters

By numerical simulation, the radial and tangential force were obtained, so was the stiffness and damping. The results were shown in Fig. 6 to Fig. 8

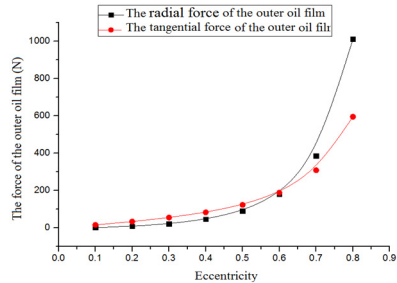
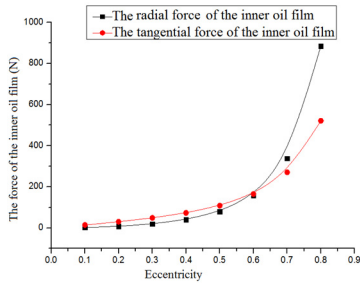


Fig. 6. The film forces versus eccentricity

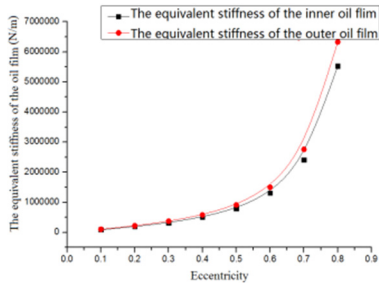


Fig. 7. The stiffness versus eccentricity

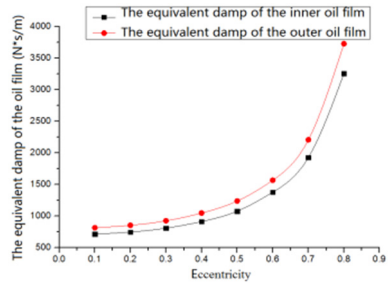


Fig. 8. The damping versus eccentricity

Basically, the forces, equivalent stiffness and damping increased with the eccentricity, as shown in Fig. 6 to Fig. 8. Under the same eccentricity, the forces of the outer oil film were larger than those of the inner oil film. When eccentricity  $\geq 0.5$ , strong nonlinear phenomenon were observed.

With eccentricity = 0.4, the influence of the radial clearance was studied. The results were shown in Fig. 9-11.

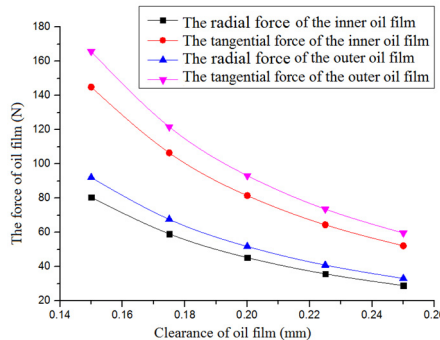


Fig. 9. The oil film force versus radial clearance

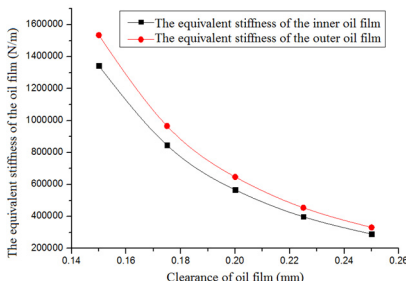


Fig. 10. The stiffness versus radial clearance

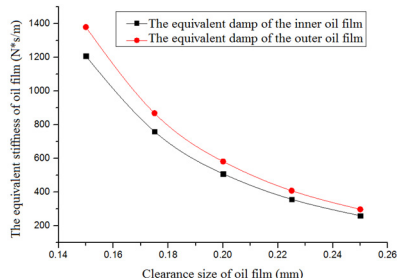
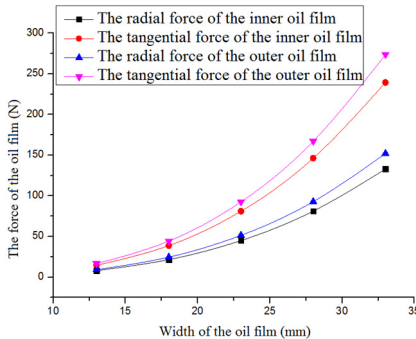


Fig. 11. The damping versus radial clearance

The forces, equivalent stiffness and damping decreased with increase of the radial clearance, as shown in Figs. 9-11. The forces of the outer oil film were larger than those of the inner oil film. The equivalent stiffness and equivalent damping of outer oil film were larger than those of the inner oil film.

Besides the radial clearance and eccentricity, influence of the width of the oil film was studied. The results were shown in Figs. 12-14.



**Fig. 12.** The oil film force versus the width of the oil film

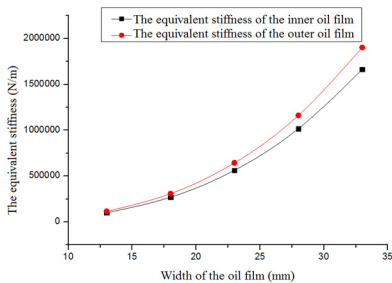


**Fig. 13.** The stiffness versus the width

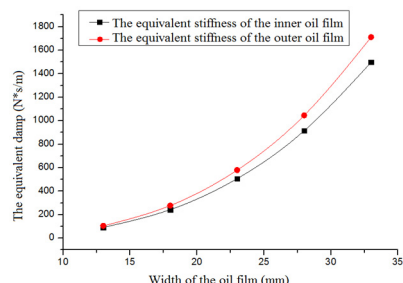
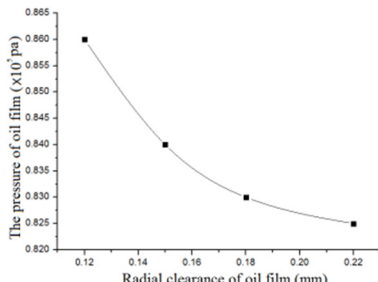


**Fig. 14.** The damping versus the width

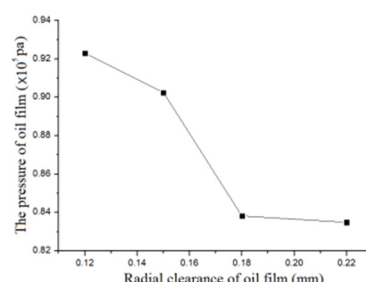
From Fig. 12 to Fig. 14, following conclusions can be reached: the forces, equivalent stiffness and equivalent damping increased with width of the oil film. The forces of the outer oil film were larger than the forces of the inner oil film. The equivalent stiffness and equivalent damping of outer oil film were larger than those of the inner oil film.

#### 4. Experiments

Experiments were conducted to validate the numerical simulation results. Only the outer film pressure was measured in the experiments. The result were shown as Fig. 15 and 16.

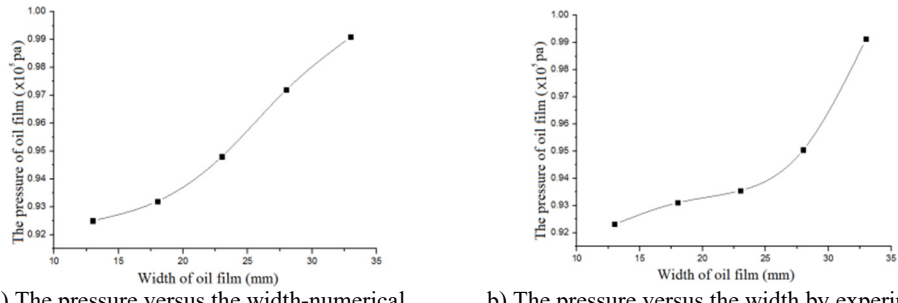


a) The pressure versus clearance-numerical



b) The pressure versus clearance-experimental

**Fig. 15.** The force versus radial clearance



a) The pressure versus the width-numerical      b) The pressure versus the width by experiment

**Fig. 16.** The force versus the width of the oil film

From Fig. 15 and Fig. 16 it can be seen that the numerical results agree well with experimental results. Both numerical and experimental research prove that the pressure of the FSFD increases with width of the oil film and decreases with radial clearance. The coincidence between numerical and experimental results also validate the effectiveness of the numerical method applied in the work.

## 5. Conclusion

In this paper, numerical and experimental researches were conducted to explore dynamic characteristics of the floating-ring squeeze film damper. The influences of the eccentricity, radial clearance and width of oil film were considered. Reynolds equations of the inner and outer oil film were derived and solved by finite difference method and SOR-Newton method to obtain pressure distribution of the oil film and thus the equivalent stiffness and damping.

By numerical search it was found that the force of the FSFD increased with eccentricity and width of the oil film due to the enhancement in squeezing. Especially when eccentricity  $> 0.5$ , strong nonlinearity between force and eccentricity was observed. Although forces of the inner and outer film followed the same pattern, force of the outer film was greater than that of the inner film with the same eccentricity. Besides, influence of the radial clearance was studied. It was found that the force decreased with increasing radial clearance, which was contrary to the eccentricity and width of oil film. Effectiveness of the numerical research was validated by experimental results.

## References

- [1] **Zhu Chang Sheng** Ability of an advanced hybrid squeeze film damper to control rotor system vibration. *Acta Aeronautica et Astronautica Sinica*, Vol. 17, Issue 2, 1996, p. 227-233.
- [2] **Hong Jie, Deng Yin, Zhang Dayi** Dynamic design method of elastic ring squeeze film damper. *Journal of Beijing University of Aeronautics and Astronautics*, Vol. 32, Issue 6, 2006, p. 649-653.
- [3] **Wen Bangchun, Gu Jialiu** Senior Rotor Dynamic. First Edition, China Machine Press, China, 2000.
- [4] **Liang Dewang**, Basic Hydrodynamics. First Edition, Aviation Industry Publishing House, China, 1998.
- [5] **Cao Lei, Gao De-ping, Jiang He-fu** Damping mechanism of elastic ring squeeze film damper. *Journal of Vibration Engineering*. Vol. 20, Issue 6, 2007, p. 584-588.